X-ray Bragg diffraction of $LiNbO_3$ crystals excited by surface acoustic waves

Rémi Tucoulou* and François de Bergevin
Laboratoire de Cristallographie, CNRS, Boîte Postale 166, 38043 Grenoble cedex 9, France

Olivier Mathon
ESRF, Boîte Postale 220, 38042 Grenoble cedex 9, France

Dimitry Roshchupkin
Institute of Microelectronic Technology, Russian Academy of Sciences, 142432 Chernogolovka, Moscow District, Russia
(Received 15 February 2001; published 12 September 2001)

This paper presents an experimental study by x-ray Bragg diffraction of a Rayleigh surface acoustic wave propagating in $LiNbO_3$ single crystals. Many parameters such as the acoustic wavelength, the acoustic amplitude, the crystal cut, and the x-ray energy were varied, thereby providing an extensive view of this acousto-optic interaction. It is shown that the diffraction spectra depend strongly on the ratio of the x-ray and acoustic penetration depths. A simple kinematical model has been developed to analyze quantitatively the acoustic fields. High-resolution x-ray diffraction seems to be a promising technique for the analysis of penetration depths of acoustic waves.

DOI: 10.1103/PhysRevB.64.134108 PACS number(s): 61.10.Nz, 77.65.Dq

I. INTRODUCTION

The development of electronic devices based on surface acoustic waves (SAW's) has been very active in the fields of filters, oscillators, real-time processing systems, and convolvers, etc., which are widely used in new communication systems (mobile phones, pagers, radio systems, TV, GPS). This development is accompanied by an increasing need for precise characterization of the acoustic fields in these devices. Interactions between x rays and SAW's have already been investigated for many years.[1–10] The development of intense third generation synchrotron sources has allowed highly parallel x-ray beams to be combined with high-resolution diffraction techniques, thus improving the experimental resolution. Recently, it has been possible to observe at the ESRF SAW-induced diffraction satellites in a Bragg geometry setup in $LiNbO_3$, GaAs, and in silicon.[11–13]

One of the main interests of such an experiment is to use x rays to probe acoustic fields in materials. For this purpose, models describing the x-ray/SAW interaction have to be developed and compared to experimental data. We have therefore carried out a systematic experimental study of x-ray diffraction by a SAW propagating in a $LiNbO_3$ crystal by varying successively the acoustic amplitude, the acoustic frequency, the crystal cut, and the x-ray energy. In a second step, we propose a simple model based on the kinematical approximation in order to derive acoustic parameters such as the amplitude and the penetration depth of the SAW inside the crystal.

II. THE SAW DEVICES

Acoustic waves of Rayleigh type were produced on SAW delay lines of conventional geometry by photolithographically deposited IDT's upon perfect $LiNbO_3$ crystals.[14] $LiNbO_3$ is one of the piezoelectric materials with the highest electromechanical coupling and is therefore largely used as a substrate in SAW-based industrial applications. We have used various conventional cuts of $LiNbO_3$ crystals: *YX*, *YZ*, [corresponding to (030) orientation], $YZ+127°$ (104), and an asymmetric cut. Acoustic wavelengths from 4 to 100 μm were used (see Table I).

Rayleigh waves are elliptically polarized, but in specular Bragg geometry, longitudinal displacements (parallel to the acoustic wave vector K yet perpendicular to the diffraction vector) do not affect x-ray diffraction. Therefore a Rayleigh wave can be approximated as a sinusoidal modulation normal to the diffracting atomic planes (see Fig. 1).

The propagation of a Rayleigh wave at the surface of a crystal induces deformations in the bulk far below the surface. Calculations have shown that the acoustic penetration should extend to a depth of the order of an acoustic wavelength.[15]

Since the phase velocity of the acoustic wave (3780 ms^{-1} for an *Y-X* cut of $LiNbO_3$) is much lower than the speed of the x rays, the acoustic deformation can be considered as quasistatic and characterized by its wavelength and amplitude. Assuming an exponential damping of the acoustic amplitude in the bulk, the vertical displacements of atoms of coordinates (x,y,z) can be written approximated as

$$H(x,z)=H_0\exp(-\mu_{ac}z)\exp(iKx), \tag{1}$$

with μ_{ac}^{-1} the penetration depth of the acoustic wave and K the acoustic wave vector. The acoustic amplitude H_0 at the surface of the crystal could be varied from 0 to a few angstroms (estimated from the number of diffraction satellites, see below) by varying the voltage supplied to the transducer.

It should be noted that we assume that the atomic planes in the crystal are distorted by the SAW but that the d spacing between them is not modified.

III. $LiNbO_3$ CRYSTAL PROPERTIES

Lithium niobate belongs to the $R3c$ space group, with a hexagonal unit cell ($a=0.51494$ nm; $c=1.3862$ nm). The d spacing of the (030) reflection (used mostly in our experi-

TABLE I. Experimental parameters of the samples used for this experiment. $\delta\alpha$: angle between two adjacent satellites in rocking curves. μ_{ac}^{-1} is calculated from the relation $\mu_{ac}^{-1} \approx 1.3\,\Lambda$.

Sample	Acoustic wavelength (μm)	Acoustic frequency (MHz)	Diffraction planes (hkl)	$\delta\alpha$ (μrad)	Energy (keV)	μ_x^{-1} (μm)	μ_x^{-1}/μ_{ac}^{-1}
a	30	116	(030)	5	13	14.5	0.37
b	12	292	(030)	12.3	8	6.0	0.38
b	12	292	(030)	12.3	10	9.0	0.58
b	12	292	(030)	12.3	13	14.5	0.93
b	12	292	(030)	12.3	15	18.5	1.19
b	12	292	(030)	12.3	18	25.6	1.64
b	12	292	(030)	12.3	20	4.6	0.29
c	12	292	(030) + 20.2°	13.1	10	3.2	0.20
d	4	952	(104)	68.2	12	6.7	1.29
d	4	952	(208)	136.5	12	13.4	2.58

ment) for $LiNbO_3$ is $d = 1.487$ Å. Based on kinematic diffraction theory, the profile of the x-ray penetration depth due to absorption in $LiNbO_3$ as a function of energy $\mu_x^{-1}(E) = \sin(\theta_B(E))/2\mu_L(E)$ is plotted in Fig. 2 (μ_L is the linear absorption coefficient; θ_B is the incident Bragg angle). It has to be noted that it varies roughly between 10 and 30 μm, which is comparable to the acoustic penetration depth. The presence of the *K* edge of Nb at 18.99 keV introduces a sharp variation (80%) of μ_x^{-1} in this region.

Considering that $LiNbO_3$ is a nearly perfect crystal when not excited, dynamical theory should then be taken into account and gives an extinction length varying between 2 and 4 μm for the (030) reflection in the 8–25 keV energy range.

IV. THE X-RAY/SAW INTERACTION

Coherent x-ray diffraction on the modulated atomic planes leads to the formation of satellites on both sides of the Bragg peak along which constructive interferences induced by the SAW occur. In the symmetric Bragg case, these angular directions can be deduced from the grating equation:

$$\cos\theta_m = m\frac{\lambda}{\Lambda} + \cos\theta_0, \tag{2}$$

with λ the x-ray wavelength, Λ the acoustic wavelength, θ_0 the incident angle, m the diffraction order, and θ_m the exit angle of the mth order satellite.

In absence of any lattice perturbation, dynamical theory is required for quantitatively analyzing the diffraction spectrum in a perfect crystal. The deformations induced by an acoustic excitation may strongly disturb the crystal, involving a progressive evolution of the dynamic behavior into a kinematic one. Since the excited acoustic field can be quite strong in our case, we have developed a very simple kinematic model predicting the diffraction satellite intensities as a function of the acoustic amplitude.[16]

The amplitude $A(Q)$ of the x-ray diffracted wave is proportional to

$$A(\mathbf{Q}) \propto \sum_{i=1}^{N} F_{hkl}(\mathbf{Q}) \exp(i\mathbf{Q}\cdot\mathbf{r}_i), \tag{3}$$

with N the number of unit cells, r_i the depth from the surface of cell i,Q the momentum transfer vector, and F_{hkl} the structure factor.

Due to the very large acoustic period with respect to the unit cell, one can assume that the variations of the structure factor are negligible when a SAW propagates. Unit cells move but are barely distorted ($\Delta d/d \sim 10^{-4}$). The position of the unit cell i can be written $r_i = r_{i0} + u(r_{i0})$ with r_{i0} the position of the unit cell in the non excited crystal. Eq. (3) becomes

$$A(\mathbf{Q}) \propto \sum_{i=1}^{N} \exp(i\mathbf{Q}\cdot[\mathbf{r}_{i0} + \mathbf{u}(\mathbf{r}_{i0})]). \tag{4}$$

According to Eq. (1), and introducing the x-ray absorption coefficient μ_x, $A(Q)$ can be written

$$A(\mathbf{Q}) \propto \sum_{x=1}^{N_x}\sum_{z=1}^{N_z} e^{-\mu_x zd} e^{i[q_x xa + q_z(zd + H(xa,zd))]}, \tag{5}$$

with N_x and N_z, the number of unit cells in the x and z direction, a the unit cell size in the x direction, $(q_x,0,q_z)$ the coordinates of vector Q.

Using the mathematical relation

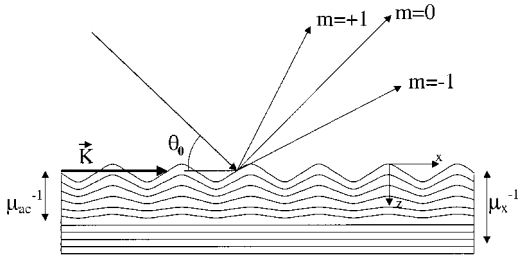

FIG. 1. Scheme of the atomic planes distorted by the acoustic wave. The z scale is multiplied by a factor 10^4 with respect to the x one. Only a few planes are represented.

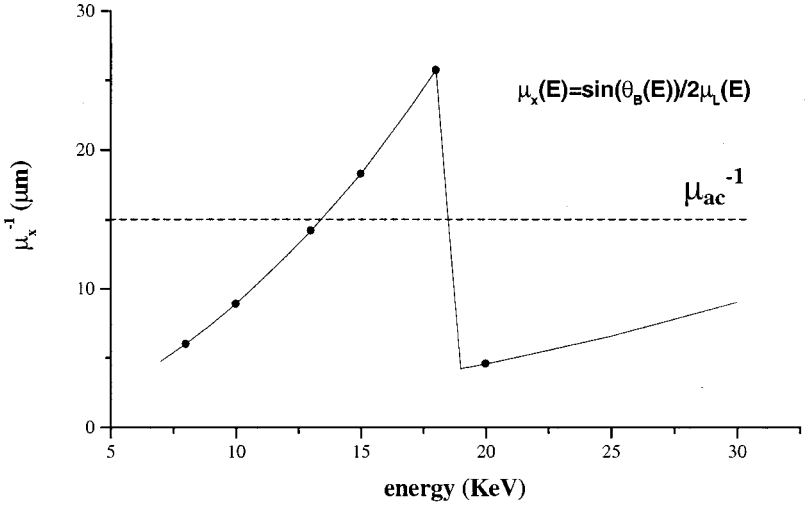

FIG. 2. X-ray penetration depth in a $LiNbO_3$ crystal vs energy. The black circles show the energies chosen for the experiment. The dotted line shows the theoretical value of μ_{ac}^{-1} for a $\Lambda = 12\,\mu$m Rayleigh wave.

$$e^{iq_z H_0 e^{-\mu_{ac} z}\sin(Kx)} = \sum_{m=-\infty}^{m=+\infty} J_m(H_0 q_z e^{-\mu_{ac} z}) e^{imkx} \qquad (6)$$

(J_m are the Bessel functions), we have

$$A(\mathbf{Q}) = \sum_m \sum_{x=1}^{N_x} e^{i(q_x+mk)xa} \sum_{z=1}^{N_z} e^{-\mu_x zd} e^{iq_z zd} \times J_m(H_0 q_z e^{-\mu_{ac} zd}). \qquad (7)$$

For $N_x \gg 1$, the first term is equal to 0 except for $q_x + mK = 0$ which is the grating equation. Finally, the mth order satellite intensity is proportional to

$$I_m \propto \left| \int_0^\infty e^{-\mu_x z} J_m(H_0 q_z e^{-\mu_{ac} z}) dz \right|^2. \qquad (8)$$

Each satellite intensity can be therefore easily calculated from the acoustic amplitude at the surface and from the acoustic and x-ray penetration depths.

V. EXPERIMENTAL SETUP

The experiment described in this paper was carried out on the triple axis diffractometer of the optics beamline (BM05) at the ESRF. The theoretical mechanical resolution is 0.5 μrad for each rotation of the goniometers. Both the monochromator and the analyzer were Si (333) crystals ($\Delta\lambda/\lambda \sim 10^{-6}$). We used a Cyberstar NaI scintillation counter for the detection. The beam was collimated by slits of 50 $\times$ 100 μm (horizontal gap $\times$ vertical gap).

VI. EXPERIMENTAL RESULTS

The first parameter which has been varied is the acoustic amplitude. Figure 3 shows several rocking curves of the $LiNbO_3$ (030) reflection from a *YX*-cut crystal recorded for various acoustic amplitudes for a wavelength of 12 μm and at a fixed energy of 13 keV.

It can be seen that the number of visible diffraction satellites increases with the acoustic amplitude. The acoustic amplitude H_0 at the surface is estimated from the number N of

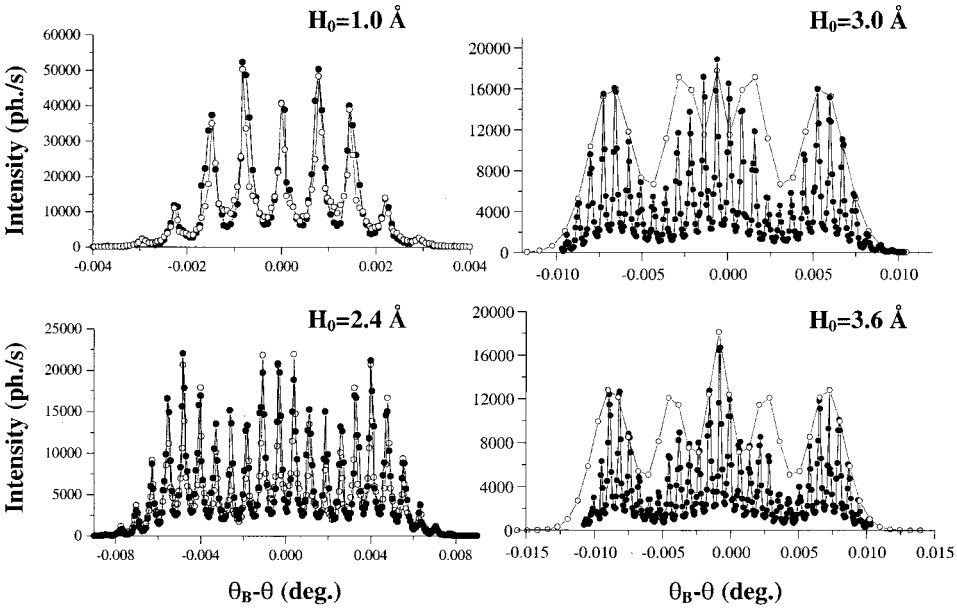

FIG. 3. Rocking curves measured (solid circles) and calculated (open circles) for 4 different acoustic amplitudes. $E = 13$ keV; $\Lambda = 12\,\mu$m; *YX* (030) reflection. To clarify the figure, the calculated rocking curves are not fully represented for the two highest amplitudes. In these cases, only the peak intensity of each satellite is shown and the line between points is only a guide for the eyes.

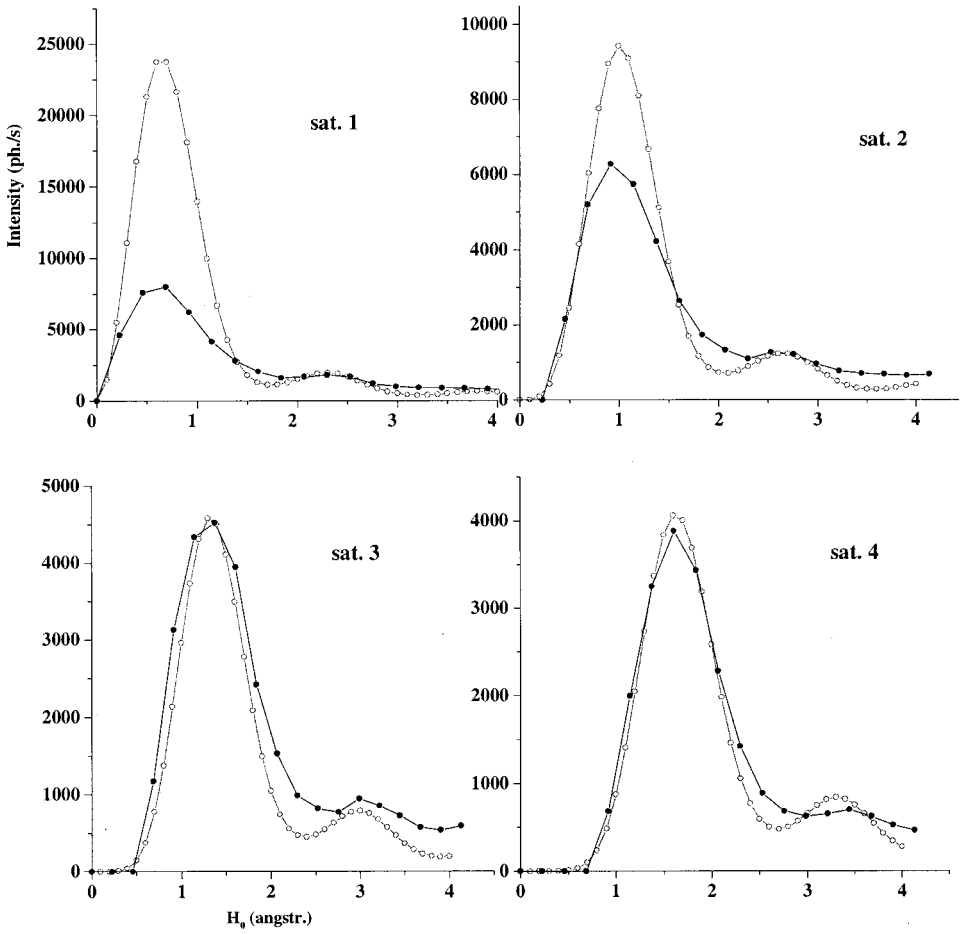

FIG. 4. Intensities of the (1,2,3,4) diffraction satellites vs the acoustic amplitude at the surface H_0. Open circles: calculated data; solid circles: experimental data. $E=13$ keV; $\Lambda=12\ \mu$m; *YX* (030) reflection.

satellites using the formula $H_0 \sim Nd/2\pi$ (the angle between adjacent satellites is d/Λ and the maximum angular deformation of the crystal is $H_0 K$).[13] Acoustic amplitudes below 0.25 Å can be detected through the rise of the $+/-1$ order satellite.

The linearity of the response of the transducer can be checked by this means. We obtain a good linearity with a ratio of 0.02 Å/mV (before a 33 dB amplifier) over a range of more than 110 mV.

The angular deviation $\delta\alpha$ between adjacent satellites is 12.5 μrad which corresponds well to the calculated value $\delta\alpha = d/\Lambda = 12.3\ \mu$rad. The FWHM of each satellite is the same as the one of the Bragg peak without ultrasonic excitation.

Figure 4 shows the variations of several successive satellites as a function of the acoustic amplitude at the energy of 10 keV. A particular satellite is observed only if the acoustic amplitude is above a threshold value, which increases with the diffraction order. Once the acoustic amplitude exceeds this threshold, the satellite intensity increases rapidly, reaches a maximum and then decreases with smooth oscillations down to an asymptotic value (see below for the interpretation).

Secondly, the same sample [*YX* $LiNbO_3$ (030), $\Lambda = 12\ \mu$m, $H_0 \sim 4.5$ Å] has been studied by recording rocking curves at several x-ray energies from 8 to 20 keV to analyze the influence of the ratio μ_x^{-1}/μ_{ac}^{-1} on the diffraction curves (see Fig. 5). At 8 keV, the FWHM of a satellite (11.3 μrad) is of the same order than the angular deviation between two of them (12.4 μ rad). This explains why the satellites are not so nicely resolved as in the other cases. Above 20 keV, the instrumental resolution of the triple-axis diffractometer was not good enough to resolve well the shape of the satellites.

One can also see in Fig. 5 that the envelope of the rocking curves varies significantly with the μ_x^{-1}/μ_{ac}^{-1} ratio. In case of small x-ray absorption (typically $E \sim 18$ keV), there is a clear predominance of the zero order peak. In case of strong x-ray absorption ($E<13$ keV or $E>20$ keV), the relative intensity of the 0 order can be very small and two symmetric maxima grow at the limits of the rocking curve for high-order satellites (see below for the interpretation).

Varying the μ_x^{-1}/μ_{ac}^{-1} ratio can also be performed by changing the acoustic wavelength ($\mu_{ac}^{-1} \sim 1.3\Lambda$ for a Rayleigh wave). We have therefore studied several acoustic devices of wavelengths 30, 12, 4 μm at the same x-ray energy (13 keV). Results are presented in Fig. 6 (except for 12 μm; see Fig. 3). For the 30 μm case [*YZ* cut (030)], the satellites are not well separated since their FWHM ($\sim 3.6\ \mu$rad) is equivalent to the angle between two of them ($d/\Lambda \sim 5\ \mu$rad). The SAW penetrates deeper than the x rays ($\mu_x^{-1}/\mu_{ac}^{-1} \approx 0.37$). Even if the satellites cannot be resolved, the envelope shows clearly that low-order satellites are weak.

In the opposite case of a large x-ray penetration depth

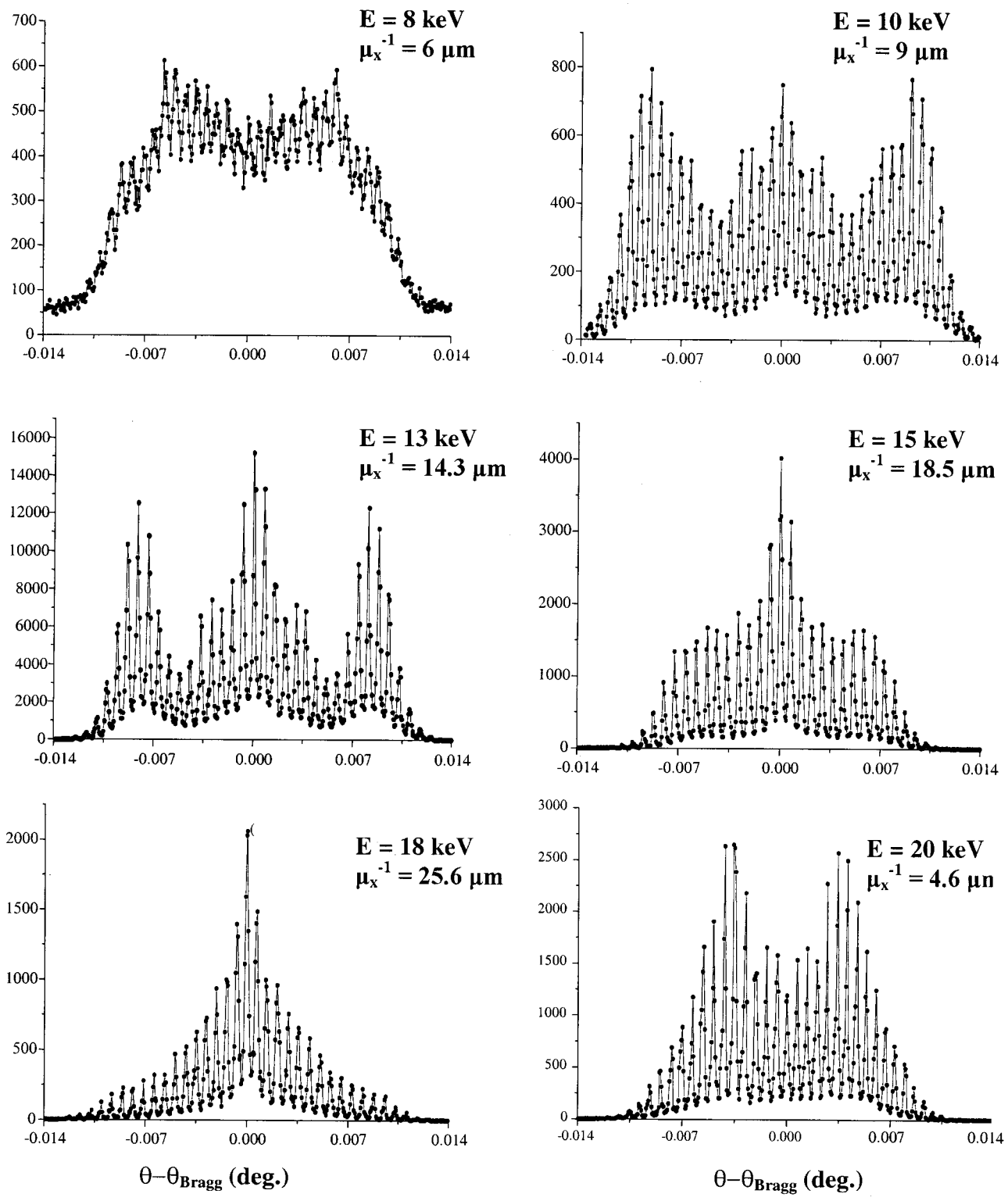

FIG. 5. Rocking curves measured for different energies. $\Lambda = 12\,\mu$m; *YX* (030) reflection; $H_0 \sim 4.5$ Å.

with respect to the acoustic one [$\Lambda = 4\,\mu$m, $YZ+127°$ (104), Fig. 6] ($\mu_x^{-1}/\mu_{ac}^{-1} \approx 1.5$), the low-order satellites prevail. In the intermediate case of $\Lambda = 12\,\mu$m [*YZ* cut (030), Fig. 3] the zero order peak and the high-order satellites have approximately the same intensity ($\mu_x^{-1}/\mu_{ac}^{-1} \approx 0.9$).

In order to confirm the dependence of the rocking curve profiles with the x-ray penetration depth, we have measured rocking curves around the (104) and (208) reflection of a $LiNbO_3$ crystal for an energy of 12 keV and an acoustic wavelength of 4 μm and an amplitude of 4.3 Å (see Fig. 7). The x-ray penetration depth is the only parameter which varies between these two cases: 6.7 μm for the (104) and 13.4

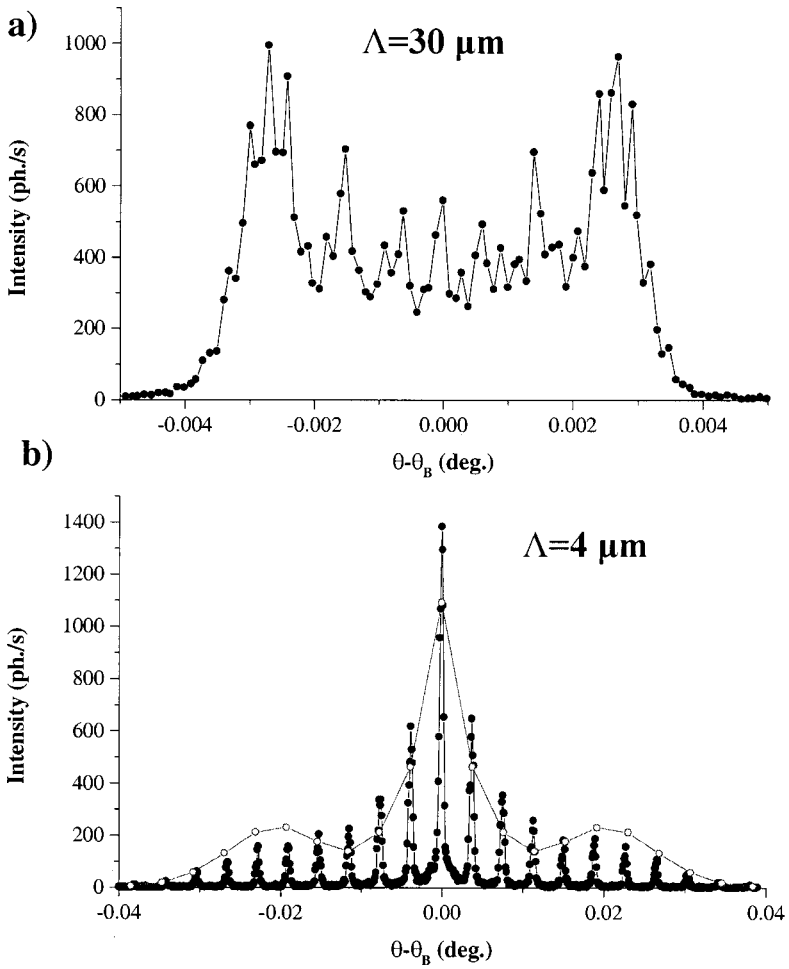

FIG. 6. Comparison between measured rocking curves for different acoustic wavelengths. $E=13\,\mathrm{keV}$. See Fig. 3 for the $\Lambda=12\,\mu\mathrm{m}$ wavelength. (a) and (b): *YZ* cut (030); (c): *YZ* $+127°(104)$. Open circles: calculated values.

for the (208). As expected, there is a large predominance of the zero order peak in the (208) case: The ratio $I_{\mathrm{sat0}}/I_{\mathrm{sat1}}$ varies from 2 (104) to 13 (208).

The last way of varying the $\mu_x^{-1}/\mu_{\mathrm{ac}}^{-1}$ ratio is to use asymmetrically cut crystals to reduce the incident angle and therefore the depth probed by x rays. The longitudinal displacements of atoms have then to be taken into account since they modify the *d* spacing between atomic planes. We have studied a $LiNbO_3(030)$ crystal with an asymmetry angle of 20.2° ($b=-0.11$). At 10 keV (incident angle$=4.28°$), the x-ray penetration depth limited by absorption is of the order of 3.2 μm ($\mu_x^{-1}/\mu_{\mathrm{ac}}^{-1}\approx 0.2$). In this extreme case, the amplitude of the acoustic field probed by x rays remains quite homogenous and x rays do not interact with static regions of the crystal. Figure 8 shows that the oscillations in the satellite intensities versus the acoustic amplitude are enhanced with respect to the symmetric case (Fig. 4). It should be noted that the zeroth order peak nearly vanishes for an acoustic amplitude of 0.7 Å.

VII. QUALITATIVE INTERPRETATION

We develop here a qualitative model allowing the global shape of a rocking curve to be understood. It does not take into account multiple beam scattering. The reader is again referred to Fig. 1 for a schematic of the damped sinusoidal SAW and the x rays. A satellite exists at a certain incident and exit angle only if there are regions of the excited crystal that stay in Bragg position and diffract in phase. For example, the extrema of the sinusoide contribute to the zeroth order satellite but only when the Bragg conditions are fulfilled for the atomic planes of these regions (i.e., for the Bragg angle of the unperturbed crystal). Similarly, the region located in $x=\pm\Lambda/2$ contributes to the highest order satellite since the slope is maximum here.

The volumes of these regions are correlated to the intensities of the corresponding satellites. This qualitative model is therefore simply based on the approximate determination of the volumes of these regions. It is clear that the position and the extension of the region indexed to a specific satellite of the rocking curve vary with the acoustic amplitude.

To approximate the volumes of these regions, it is necessary to take into account the x-ray penetration depth and more precisely the ratio $\mu_x^{-1}/\mu_{\mathrm{ac}}^{-1}$. If the x-ray penetration depth is larger than the acoustic one, x rays can reach deep regions where the crystal remains static and nondistorted as Fig. 9 illustrates. In this case, the region contributing to the zeroth order satellite can become very large compared to regions of higher orders. When the zeroth order satellite becomes predominant, it is the signature of a large x-ray penetration depth with respect to the acoustic one (see 18 keV in Fig. 5). On the other hand, if μ_x^{-1} is small compared to the

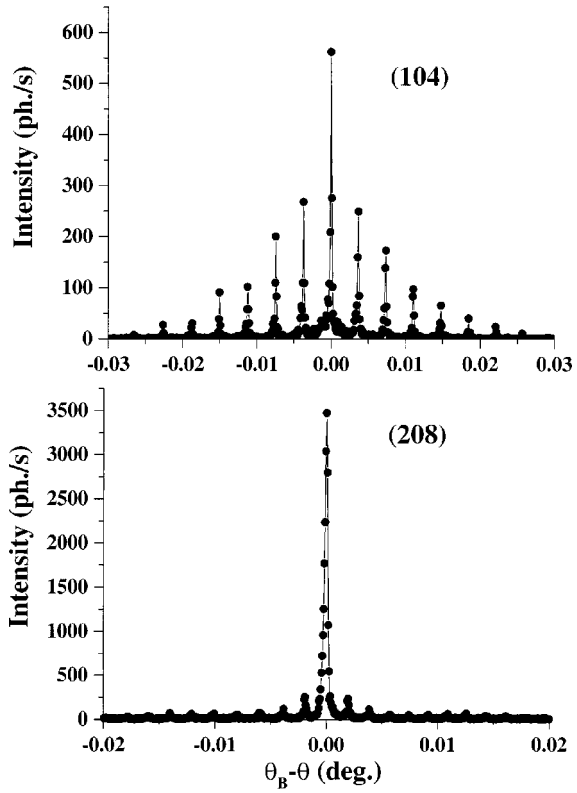

FIG. 7. Comparison between rocking curves recorded around the (104) reflection (open circles) and (208) reflection (solid circles). $E=12$ keV; $\Lambda=4$ μm.

acoustic penetration depth, each diffracting region contributing to a specific satellite reaches approximately the same depth (μ_x^{-1}) in the bulk and their respective volumes are roughly proportional to their size along the x direction (see 20 keV in Fig. 5).

This size can be estimated by convoluting the acceptance of the crystal ω_D with the local slope variations of the sinusoidal shape of the atomic planes, as follows. The sinusoidal SAW has nodes at $x=0$ and at $x=\Lambda/2$ where the displacement is zero, the slope variation is maximum $[|d^2z/dx^2|=H_0K^2\sin(Kx)]$, and the slope variation is close to zero. Due to the large slope, these regions contribute to high-order satellites. Due to the small slope variation, these regions have a large area. This explains why some extrema are visible for high-order satellites in case of small x-ray absorption (see 8, 10, or 20 keV in Fig. 5).

We have seen that in order to explain qualitatively the rocking curve profiles, it is useful to identify local regions which diffract both specularly and in phase for a specific incident beam. For any incident angle between ($\theta_{\mathrm{Bragg}}-H_0K$) and ($\theta_{\mathrm{Bragg}}+H_0K$), each period provides two different regions that satisfy the criteria of specular reflection (for example maxima and minima regions for the zeroth order). Constructive interferences of the x rays are therefore also possible: For the zeroth order beam for example, if the acoustic amplitude H_0 is equal to $d/2$, then the difference in height between maxima and minima is d, and therefore these regions diffract in phase, and the zero order intensity should be enhanced. In addition, it induces a virtual periodicity of

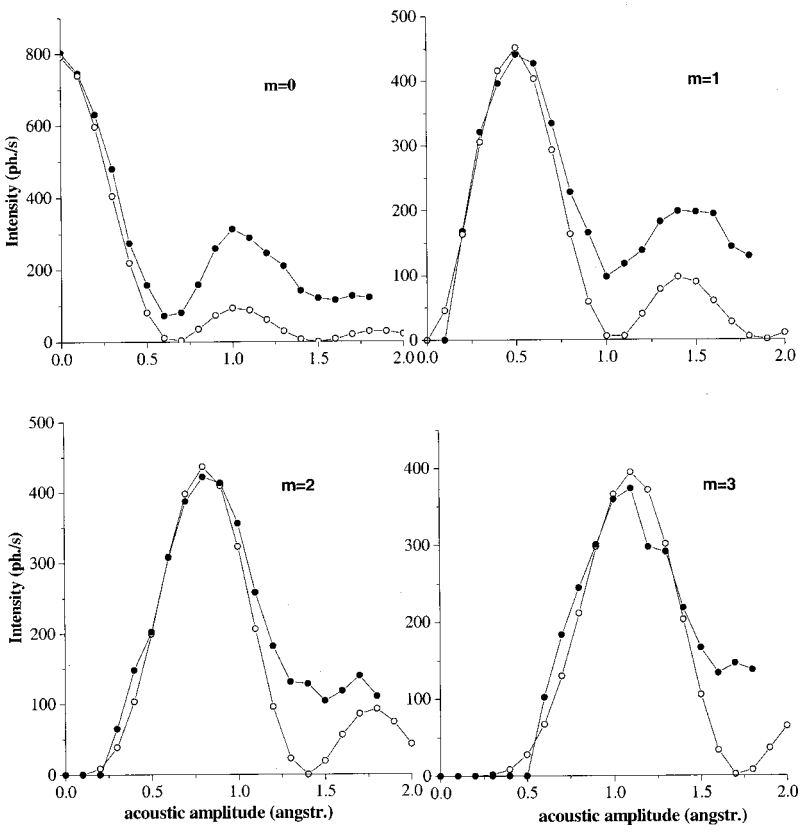

FIG. 8. Intensities of the (0,1,2,3) diffraction satellites vs the acoustic amplitude at the surface H_0. Open circles: calculated data; solid circles: experimental data. $E=10$ keV; $\Lambda=12$ μm; asymmetric reflection.

$\Lambda/2$ instead of Λ. The $+/-1$ order satellites should therefore appear at the usual $+/-2$ order positions. It can be seen on Fig. 8 where the maximum of the 0 order corresponds to a minimum of the $+1$ order (and to a maximum of the $+2$ order). This phenomenon can explain why some oscillations are observed in Fig. 4 and Fig. 8. They are clearly stronger in the asymmetric case where the whole diffracting volume participates to this phenomenon since the acoustic absorption is nearly negligible. In the symmetric case, this effect is attenuated by contributions from deep regions in the crystal where the acoustic amplitude is much lower than H_0 at the surface.

VIII. KINEMATICAL SIMULATIONS

Since Rayleigh waves are well known, simulations can test the validity of the kinematic model. Most of the rocking curves presented in the experimental results are simulated. The position (Q_x direction) of the satellites is deduced from the grating equation [first part of Eq. (7)], the satellite FWHM is deduced from the static Bragg peak and the satellite peak intensity is calculated from Eq. (8). H_0 is preevaluated from the equation $H_0 \approx Nd/2\pi$.[13]

For the clarity of the figures, a satellite is sometimes only represented as its peak intensity at the calculated angular position. The only parameters which were varied are the acoustic amplitude H_0 and the acoustic penetration depth μ_{ac}^{-1}.

It can be seen in Fig. 3 (open circles) that the number of satellites and the global shape of the envelope are correctly predicted in case of $\mu_x^{-1}/\mu_{ac}^{-1} \sim 1$ ($E=13$ keV; $\Lambda=12\ \mu$m; $\mu_x^{-1}/\mu_{ac}^{-1} \sim 0.95\ \mu$m). Calculations give an acoustic penetration depth of $\mu_{ac}^{-1} \sim 13\ \mu$m ($\pm 0.5\ \mu$m), i.e., $\mu_{ac}^{-1} \sim 1.1\Lambda$ which is consistent with the theoretical value ($1.3\ \Lambda$).

The results are even better when $\mu_x^{-1}/\mu_{ac}^{-1} < 1$ as for the asymmetric crystal case (see Fig. 8, $\Lambda=12\ \mu$m, $E=10$ keV, $\mu_x^{-1}/\mu_{ac}^{-1} \sim 0.2$). These kinematic simulations predict in both cases the period and the position of the oscillations in the intensity of the satellites versus the acoustic amplitude.

In case of $\Lambda=4\ \mu$m and $E=13$ keV [(104) reflection], $\mu_x^{-1}/\mu_{ac}^{-1} \sim 1.5$, the simulation is not too bad (see Fig. 6) predicting $\mu_{ac}^{-1} \sim 4.6\ \mu$m ($\pm 1\ \mu$m). The theoretical value is $5.2\ \mu$m.

As soon as x rays meet some nondistorted regions inside the crystal ($\mu_x^{-1}/\mu_{ac}^{-1} > 1$), the kinematical model does not give good results because it often overestimates the zeroth order peak [see $E=18$ keV, (030) reflection, $\Lambda=12\ \mu$m, $\mu_x^{-1}/\mu_{ac}^{-1} \sim 1.7$]. This is not surprising since static regions require dynamic theory. In case of silicon crystals,[13] the kinematic model is useless. If x rays are used to probe the acoustic field in a material, kinematical simulations can be used as long as the x-ray energy is set to satisfy the criteria $\mu_x^{-1}/\mu_{ac}^{-1} < 1$. It has to be noted that the shape of the envelope of a rocking curve provides nevertheless a good estimation of the μ_x^{-1}/μ_{ac}^{-1} ratio.

We have experimentally observed that many parasitic effects may influence the diffraction spectra such as the bulk acoustic wave simultaneously emitted by the transducer and the nonhomogeneity of the acoustic amplitude induced by acoustic diffraction or crystal defects. These effects could not be captured by the simulation model.

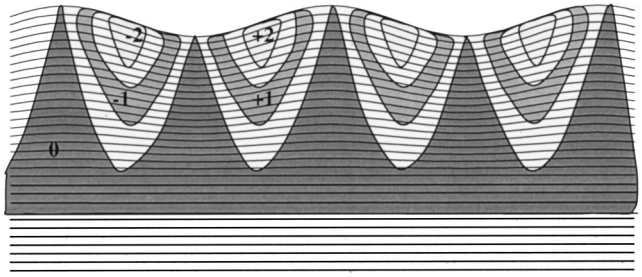

FIG. 9. Schematic visualization of regions of the excited crystal diffracting into successive satellites in case of small x-ray absorption. The white regions diffract in antiphase and do not contribute to any satellite. The z scale is multiplied by a factor 10^4 with respect to the x one. Only a few planes are represented.

IX. CONCLUSION

A Rayleigh wave propagating at the surface of a crystal induces satellites in the diffraction pattern which can be resolved using high-resolution x-ray diffraction techniques. It has been shown experimentally that the profile of the rocking curves depends essentially on the ratio μ_x^{-1}/μ_{ac}^{-1} of the x-ray and acoustic penetration depths. A simple kinematical model has been developed to simulate the measured diffraction pattern and to retrieve acoustic parameters from the diffraction patterns. It provides some correct results if x rays do not penetrate to the deep undistorted regions inside the crystal. For the (030) reflection in $LiNbO_3$, and an acoustic wavelength of $12\ \mu$m, the x-ray energy should be lower than 13 keV. But below 10 keV, the FWHM of satellites becomes too large and they cannot be separated.

The development of a dynamical model is under progress and should provide better results than the kinematical one, especially in case of small acoustic amplitudes and/or large x-ray penetration depths.

To our knowledge, x rays are the only probe allowing a direct measurement of the acoustic fields in crystals. This kind of experiment could be helpful in the confirmation of theoretical calculations of the acoustic penetration depths for example. Rayleigh waves are well described by theoretical models but there exists many others types of acoustic waves (high velocity pseudo surface acoustic waves for example) still under study today and which could be characterized with x rays.

ACKNOWLEDGMENTS

We thank K. F. Peters for a critical reading of the manuscript. This work has been supported by a joint program between the CNRS and the IMT in Chernogolovka. One of us (D.V.R.) is indebted to the Russian Foundation for basic research (Contract No. 00-02-16045).

*Author to whom correspondence should be addressed. FAX: (33)-4-76-88-10-38. Email address: tucoulou@polycnrs-gre.fr

[1] H. Cerva and W. Graeff, Phys. Status Solidi A **82**, 35 (1984).
[2] S. Kikuta, T. Takahashi, and S. Nakatani, Jpn. J. Appl. Phys., Part 2 **23**, L193 (1984).
[3] A. R. Mkrtchyan, M. A. Navasardyan, R. G. Gabrielyan, and L. A. Kocharyan, Solid State Commun. **59**, 147 (1986).
[4] A. R. Mkrtchyan, M. A. Navasardyan, L. A. Kocharyan, K. G. Galoyan, R. G. Gabrielyan, and O. A. Unanyan, Sov. Tech. Phys. Lett. **12**, 629 (1986).
[5] D. V. Roshchupkin, M. Brunel, F. de Bergevin, and A. I. Erko, Nucl. Instrum. Methods Phys. Res. B **72**, 471 (1992).
[6] E. Zolotoyabko, B. Sander, Y. Komen, and B. Kantor, Acta Crystallogr., Sect. A: Found. Crystallogr. **A50**, 253 (1994).
[7] W. Sauer, T. H. Metzger, J. Peisl, Y. Avrahami, and E. Zolotoyabko, Nuovo Cimento D **19**, 455 (1997).
[8] D. V. Roshchupkin, I. A. Schelokov, R. Tucoulou, and M. Brunel, Nucl. Instrum. Methods Phys. Res. B **129**, 414 (1997).
[9] E. Zolotoyabko and I. Polikarpov, J. Appl. Crystallogr. **31**, 60 (1998).
[10] I. Polikarpov, R. Toledo de Oliveira, and E. Zolotoyabko, Rev. Sci. Instrum. **70**, 2230 (1999).
[11] R. Tucoulou, O. Mathon, D. V. Roshchupkin, I. A. Schelokov, and M. Brunel, *ESRF Highlights 1997/98*, edited by D. Cornejuols (1998), pp. 98, 99.
[12] W. Sauer, M. Streib, T. H. Metzger, A. G. C. Haubrich, A. Wixforth, J. Peisl, A. Mazuelas, J. Härtwig, and J. Baruchel, Appl. Phys. Lett. **75**, 1709 (1999).
[13] R. Tucoulou, O. Mathon, R. Pascal, D. V. Roshchupkin, I. A. Schelokov, E. Cattan, and D. Remiens, J. Appl. Crystallogr. **33**, 1019 (2000).
[14] R. M. White and F. W. Voltmer, Appl. Phys. Lett. **7**, 314 (1965).
[15] M. Moriamez, E. Bridoux, J-M. Desrumaux, J-M. Rouvaen, and M. Delannoy, Rev. Phys. Appl. **6**, 333 (1971).
[16] R. W. James, *The Optical Principles of the Diffraction of X-rays* (Ox Bow, Woodbridge, CT, 1947).